Book of Tutorials and Abstracts

European Microbeam Analysis Society

EMAS 2026

15th

REGIONAL WORKSHOP

TOPICAL CONFERENCE ON ELECTRON BACKSCATTER DIFFRACTION (EBSD)

14 to 17 June 2026
at the
CentraleSupélec, Gif-sur-Yvette, France

Organised in collaboration with:
ICMMO, ENS Paris-Saclay,
Université Paris-Saclay

EMAS
European Microbeam Analysis Society eV
www.microbeamanalysis.eu/

This volume is published by:
European Microbeam Analysis Society eV (EMAS)
EMAS Secretariat
c/o Eidgenössische Technische Hochschule, Department of Earth and Planetary Sciences
Clausiusstrasse 25
8092 Zürich
Switzerland

ISBN 978 90 8227 6992
NUR code: 971 – Materials Science

EBSD – AN HISTORICAL POINT OF VIEW

François Brisset

CNRS, Université Paris Saclay, ICMMO, CentraleSupélec
91400 Orsay, France
e-mail: francois.brisset@universite-paris-saclay.fr

François Brisset received his doctorate from Paris-Sud University in 1993 for his work on the chemical interface of ceramic-metal matrix composites. He then completed a postdoctoral fellowship at the University of Birmingham, specialising in mechanical strength. Following this, he worked for three years in industry, notably with EBSD technology, at a time when automatic band recognition was not yet implemented. He then joined the CNRS (French National Centre for Scientific Research) to head a transmission electron microscopy (TEM) service at ONERA (French Aerospace Lab). He is now back at Paris-Saclay University, where he leads the Microscopy and Surface Analysis group, which includes TEM, SEM, AFM, and XPS techniques. Over the years, he has participated in numerous research programmes, often related to EBSD.
As president of GN-MEBA (National Group for Scanning Electron Microscopy and Microanalysis) since 2008, he is responsible for the association's activities, which host over 200 people each year at its annual congress in Paris. He has overseen the publication of five books, including the French reference work on scanning electron microscopy and microanalysis (over 1,000 pages), a book on electron backscatter diffraction (EBSD), and another, recently published, on sample preparation. During this period, he has also organised three summer schools, bringing together approximately 200 people for a week and providing access to 18 microscopy columns equipped with their accessories.
After teaching in various university programmes, he has dedicated himself for the past ten years to continuing education and adult learning, notably at the CNRS and the CNAM, where he is responsible for several programmes while also teaching.
FB has been co-opted member of EMAS since 2009, having participated in organising EMAS 2011 in Angers.

1. INTRODUCTION

In this chapter we will trace the evolution of the electron backscatter diffraction (EBSD) technique from the observation of the very first Kikuchi lines to the most recent advances. We will review the first electron diffraction images observed in reflection mode in a chamber equipped with an electron gun and their evolution over the decades preceding the advent of the scanning electron microscope (SEM). We will then discuss the discoveries of various SEM diffraction techniques before the rise of the EBSD technique, due to its characteristics and its contribution to materials science, compared to other techniques, starting in the 1980s and its automation in 1992. Finally, we will introduce main developments, some of which are still ongoing. This paper will also cover the first steps of EBSD-energy-dispersive X-ray spectrometry (EBSD-EDS) coupling, 3D EBSD, transmission EBSD in the SEM and high-angular resolution EBSD. These later points will be developed during the workshop and detailed in other articles in the present book of abstracts.

2. THE FIRST WORKS

It all seems to have begun in 1928 when S. Kikuchi, a student of S. Nishikawa, became interested in the work undertaken by both C. Davison and G. Thomson [1, 2]. These two researchers had discovered that a cathodic beam passing through a metal film could produce a diffraction image "similar" to that produced by X-rays in a Debye-Scherrer equipment. This beam-sample-pattern assembly had thus enabled them to confirm experimentally De Broglie's hypothesis postulating that particles (such as electrons) could behave like waves (wave/particle duality 1924). Davidson and Thomson were awarded the Nobel Prize in Physics in 1937 for this work.

Thus, Kikuchi reproduces the experiment on mica and highlights, as before, by transmission the same types of patterns. However, by moving towards thicker areas of the sample, he showed that lines also appeared and then called them "patterns of the second types" and are now called Kikuchi lines (Fig. 1a) [3]; the first type of shots being the spot shots (previously mentioned). He noticed that the transition between the first and second type of patterns was continuous as the thickness of the mica increased, and that often the two types of patterns overlapped. In the same year, Kikuchi found more or less similar lines on calcite (Fig. 1b and 1c); calcite ($CaCO_3$) is a very abundant mineral that can cleave easily [4]. To obtain these new lines, the surface of the sample was no longer placed perpendicular to the beam but at a certain angle and the beam no longer passes through the sample. The photographic film was then placed opposite the surface of the sample and parallel to the direction of the beam. The images showed pairs of lines or bands which were then called fourth type images. Thus, these lines were called in different ways for a few decades, but at the present time they are generally called pseudo-Kikuchi lines or more simply Kikuchi lines (depending on the context). By comparing the bands of the photograph (Fig. 1b) with the X-ray data, the families of planes could be determined. However, the band

width was not defined sufficiently to go back to the crystal parameters. Despite all the advances and progress generated subsequently, this last point is still relevant; even if under certain conditions, it is possible to identify phases.

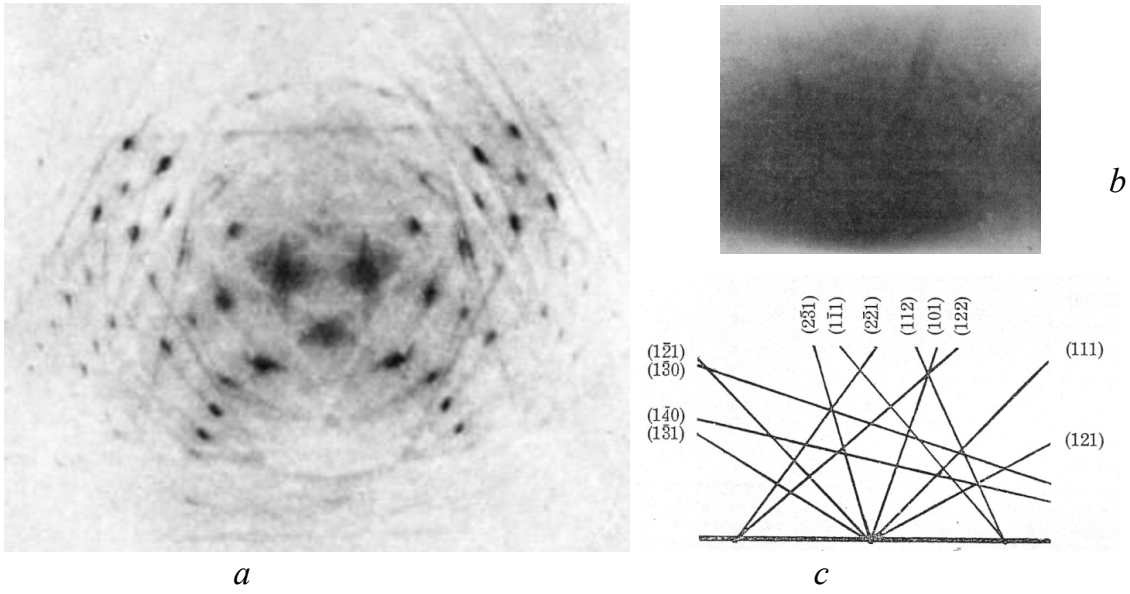

Figure 1. a) Kikuchi lines observed in transmission electron microscopy (TEM) on mica, together with spots. b) Pseudo-Kikuchi lines obtained on calcite. c) Indexation of these lines on calcite.

However, in the 1930s (and for several decades), SEM did not yet exist. These lines were actually observed using a gas-discharge electron gun (Fig. 2). In such a device, an electron beam accelerated to about 50 kV (or less) was generated in a gas discharge chamber and was directed towards a sample, possibly under a grazing incidence (a few degrees); the pattern being recorded on a photographic plate. Thus, in this type of equipment, a plasma is created by discharging gas (H_2 and O_2). The electric field between the anode and the cathode attracts ions to the cathode. Following this bombardment, electrons are emitted from the cathode and are then attracted to the anode and thus directed to the sample. It should be noted that the vacuum is quite rudimentary and there is no real separation between the gun and the sample chamber.

Following these first experiments, other authors have worked on the subject such as R. Meibom [5] and H. Boersch [6]. The latter has produced, with the help of electrons with an energy of 20 kV and photographic plates, a collection of very good quality diffraction diagrams. These were recorded from various materials, again including calcite, but also fluorite, quartz and mica, diamond, lead sulphide, potassium and chlorine chlorides, copper and iron, etc. (Fig. 3). The surfaces of these samples were cleaved or polished. Due to the high quality of these images, it was possible to verify that the bandwidth was proportional to the interlattice distance according to Bragg's law ($2d\sin\theta = n\lambda$) and that it was thus related to the energy of the electrons.

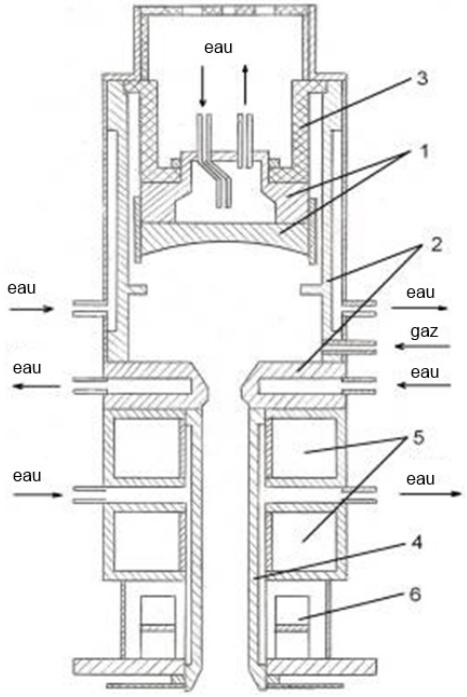

The different elements of a gas discharge gun (the sample chamber is located below and is not shown in the diagram):

1 – Cathode
2 – Anode
3 – Insulator
4 – Electron column
5 – Focussing coils
6 – Scanning coil

Figure 2. Gas discharge electron gun.

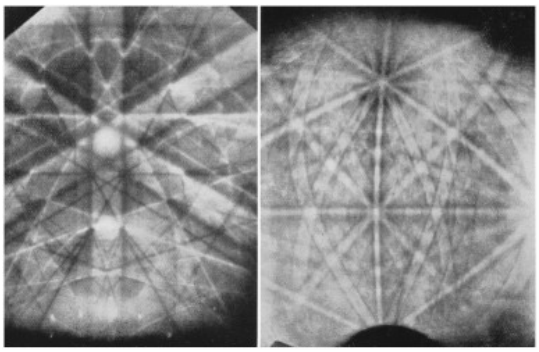

a) b)

Figure 3. Diffraction images obtained on a) iron, and b) fluorine.

A few years later, different authors tried to obtain wide-angle patterns. Thus, various experiments have been undertaken, and in particular that of M. Alam [7]. He and his colleagues have developed a special cylindrical photographic chamber that can be used to obtain wide-angle diffraction images of up to 165°, by reflecting electrons with energies ranging from 6 to 50 kV (Fig. 4).

In this chamber, the incident electrons move from A to B and the crystal is placed in C. The photographic film is marked between points D, E and F and a curved cover is placed in front of it and is marked by points G, H and K. A phosphorescent zone is located between the points

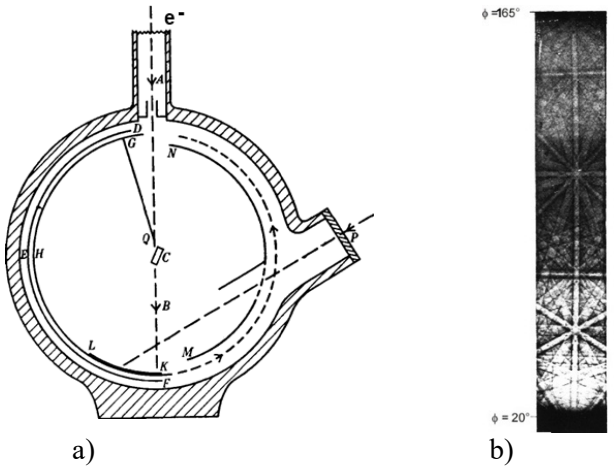

a) b)

Figure 4. a) Cylindrical photographic camera, and b) example of a wide-angle diffraction pattern.

K and L to allow the system to be adjusted by looking through the opening P. Another curved cover is placed between the M and N points in order to hide the phosphorescent area of the first cover as it rotates; it thus makes it possible not to veil the film. When shooting, the GHK cover rotates to expose the film to the electrons in order to gradually expose the film according to the deflection. The rotation speed is variable to adapt the exposure time of the film to the angle of diffusion. An example of a diffraction image obtained under these conditions is shown in Fig. 4b; it comes from a sample of lead sulphide. The observation of the diffraction images obtained by this technique showed that the bandwidth did not vary with the angle of scattering, contrary to what had been announced by some authors and depended only on the energy of the incident electrons.

3. INTRODUCTION OF THE SCANNING ELECTRON MICROSCOPE

Then, for a decade, there was little evolution and few studies in the field of electron diffraction as presented above. Then, electron diffraction underwent an evolution with the advent of the first commercial scanning electron microscope in 1965, the Cambridge MKII Stereoscan. Then, as early as 1967, Coates [8] highlighted Kikuchi lines in SEM and three groups from the universities of Oxford, Bristol and Sussex presented work on different diffraction techniques inside an SEM. Thus, respectively Joy [9], Biggin and Dingley [10], and finally Venables [11] undertook remarkable studies on the selected area channelling pattern or electron channelling pattern (SACP or ECP), Kossel diffraction (XKL) and electron diffraction (future EBSD) techniques. These works were published between 1971 and 1973. An example of diffraction images, typical of these three techniques, is shown in Fig. 5.

Venables, from the very beginning, has evolved the third technique from the point of view of data acquisition. Indeed, he modified the chamber of a scanning electron microscope to be able to use a TV camera to record patterns of different materials instead of a photographic film.

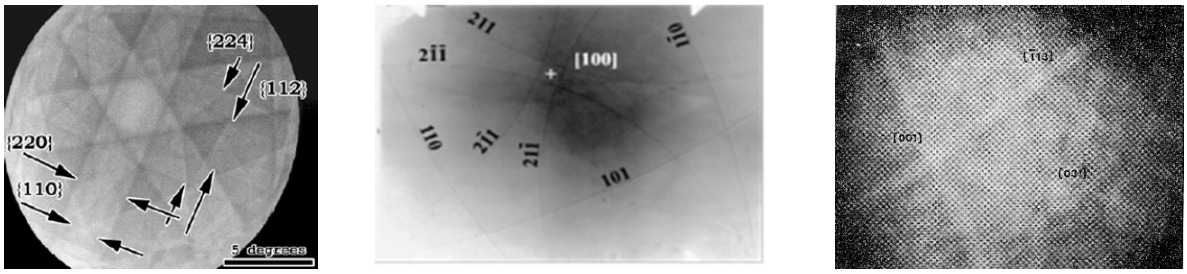

a) b) c)

Figure 5. Respectively, diffraction patterns of: a) ECP, b) Kossel, and c) EBSD.

The images obtained in this way were of lower quality, but this method of data collection offered greater interactivity. It was at this time that the initials of the technique we know today appeared. Indeed, in his article, Venables describes the images this way: "Because the patterns are so similar to ECP's and because they map the angular distribution of back-scattered electrons, we propose to call them electron back-scattering patterns and denote them by the initials E.B.S.P.". However, the group at the University of Sussex did not stop there and in order to be able to index the patterns, they used the 3-ball method developed previously for the Kossel diagrams [12], in order to determine the position of the centre of the pattern and, therefore, the crystallographic orientation (Fig. 6) [13]. The pattern centre (PC) is located at the point of intersection of the lines corresponding to the major axes of the 3 ellipses (Fig. 6a, only 2 ellipses are shown in the diagram in Fig. 6b), Z being the sample-screen distance. With the help of this method, the orientation of the crystal with respect to the sample could be determined with an estimated accuracy of 1°.

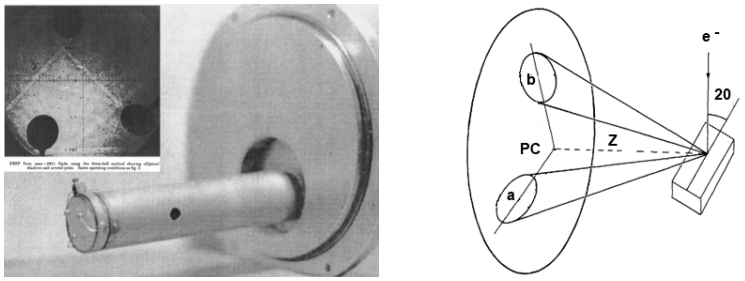

a) b)

Figure 6. a) Assembly of the 3 balls in front of a phosphorescent screen and visualisation of a pattern and the 3 balls; b) Diagram showing the position of the pattern centre (PC) [12].

Already at that time, Joy [14] and Venables [13] highlighted some advantages of electron diffraction compared to X-ray diffraction in a SEM. One of the main advantages was related to the time it took to acquire a pattern. Indeed, it could be acquired in a few seconds for electrons

but required several minutes for Kossel images. Another point was that not all elements could be observed because of the energy of the incident electrons and the excitation conditions of the emitted and diffracted X-rays according to Bragg's law.

These first observations were confirmed and supplemented, in detail, by an in-depth study conducted by Dingley in 1981 [15]. Indeed, backscattered electron diffraction has another significant advantage over the other two techniques, that of offering a much better spatial resolution for XKL and ECP it is of the order of 10 µm while an EBSP pattern comes from a much smaller area (sub-µm). Finally, ECP only allows to have a very small solid angle of diffraction, of the order of 8 to 10°, whereas EBSD allows thanks to its solid angle of around 65 - 70° to obtain several main zone axes on the same pattern and, therefore, to facilitate the indexing. Beyond these initial conclusions, it should be added that EBSP patterns can be acquired on all SEMs because they do not require tilting the electron beam in order to obtain a diagram as it is the case for ECP, which requires additional functions at the SEM column level. In addition, indexing is simpler for EBSP patterns, compared to X-ray ones, because the bands are similar to straight lines, which is not at all the case for the lines obtained on Kossel diagrams (today, this is still an issue).

4. A LEAP FORWARD

From this date (1981-1982), EBSD developed considerably. Numerous studies were undertaken by Dingley, and in particular, he demonstrated that it was possible to acquire data on sub-µm phases [16]. As a result, fully manual and laboratory systems were quickly replaced by the first commercial product capable of semi-automatically indexing EBSD patterns in 1987. To do this, a SIT (silicon intensified target) video camera coupled with an optical fibre was installed by Dingley on a SEM. It is capable of viewing a pattern on a computer screen, via a video capture card called "frame grabber" [17-18]. Once the picture is viewed, all you have to do is recognise 3 zone axes, point them on the screen and name them. Then, a programme can index the pattern and define the orientation of the crystal on its own. In order to help in the recognition of the axes of the zones, an atlas was, therefore, published [19]. In 1989, a new development made it possible to use the lines of the pattern instead of zone axes, in order to help index ECP images by N. Schmidt [20]. To do this, you have to draw the six lines corresponding to the edges of three bands to get directly the indexation. Moreover, the conclusion of this paper is that “the ECP is better than the EBSD in many cases because of the large angle of inclination of the latter technique” (70°) and this despite the lower resolution of the ECP; history has contradicted this conclusion and EBSD took over! As early as 1991, a similar method was applied to EBSD patterns by D. Jeesen [21].

The following year, in 1992, the work of S. Wright within B. Adams' group led to the emergence of the first fully automated system and the first orientation maps [22]. To achieve this state and move from a manual or semi-automatic system to a fully automatic system capable of carrying

out orientation mapping, it was necessary to be able to introduce two particular novelties. Thus, it was necessary, on the one hand, to control a movement, and on the other hand, to make the detection of Kikuchi bands automatic. Regarding the first point, a special stage, equipped with 0.1 µm precision piezoelectric motors, had been installed on a SEM. This stage could, therefore, be controlled by the acquisition programme; at the time, there was no possibility of external control of the microscopes, either for the beam or the stage. These first automatic EBSD analysis systems were, therefore, equipped with stage displacement, which was quite slow (and still is). With respect to the second point, automated software detection of zone axes or bands was required prior to the indexing process. For this first fully automated system, the detection of the bands was, therefore, carried out using Burns' algorithm [23]. Indeed, according to Burns, his algorithm seemed "more suitable for detecting and recognizing portions of low-contrast lines than Hough's algorithm" [24], especially since the latter had originally been developed for binary images. The principle of Burns' algorithm is to group linear regions and pixels with similar orientation gradients, using masks (Fig. 7a). The goal is to isolate the lines (or portions of lines) from the low-contrast images that are the pseudo-Kikuchi lines (Fig. 7b), and then to reconstruct the entire lines and borders for subsequent indexing processing (Fig. 7c). Once the bands have been detected (the bands correspond to the families of diffracting planes), the general principle of the method of indexing a pattern is to calculate the angles between the identified bands and to compare these angles with those obtained between the families of planes (hkl) of the selected phase (no multiphase analysis was available at first). When there is agreement between these angular values, a solution concerning the orientation of the given point can be validated by the programme. The system acquires the next point and step by step, the orientation mapping is carried out.

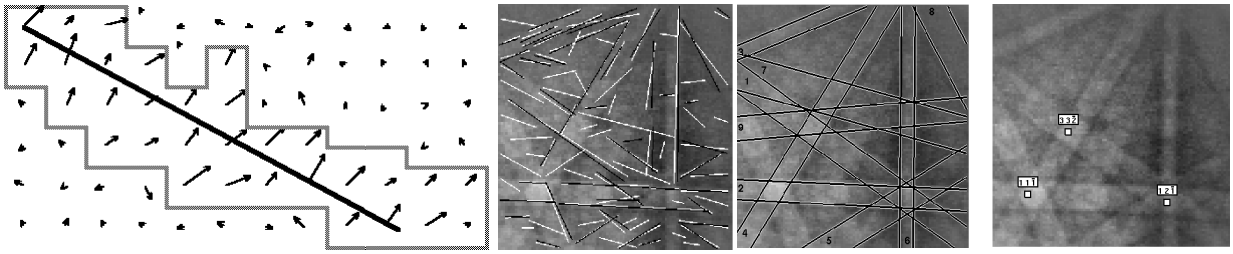

a) b) c) d)

Figure 7. a-b) Detection of groups of pixels of similar gradient; c) Reconstruction of the lines; d) Indexing, from [25].

Thus, in 1992, Stuart Wright presented the first automated system during his PhD at Yale University [25]. A computer controlled both the SIT camera and the installed stage, using a programme able to run 4 microprocessors in parallel. The data file then contained for each point acquired, the orientation (in the form of Euler angles), a parameter relating to the quality of the pattern, called IQ, and the coordinates of the point (X, Y). One of the first maps acquired is shown in Figs. 8a-8b; it is an aluminium alloy that was compressed of 40 %, the acquisition

step was 1 µm and the acquisition time of a point, including indexing, was 3 seconds. In the same year, N. Krieger-Lassen introduced the Hough transform for band detection in an EBSD pattern and it was used in parallel with the Burns transform by S. Wright in his algorithm following work he had done with Kunze [26, 27]. For about 15 years, these two detection algorithms were used in parallel in OIM-DCTM, at the user's choice. Each has some advantages depending on the situation (the Bruns' transform could sometimes be more effective in the case of very low contrast bands and the Hough transform being significantly faster). The Hough transform (currently used differently depending on the manufacturer, possibly modified), was until now the only method for indexing a pattern. The Hough transform principle involves transforming a pseudo-Kikuchi band in "real" space (Fig. 8c) into a more intense peak in Hough space (Fig. 8d) using the equation $\rho = x \cos\theta + y \sin\theta$. This transformation facilitates the band detection by summing the higher intensity pixels in the image. Once the peaks, and therefore the bands, are identified, the angles between the bands (families of planes) are compared to the angles between the families of planes of a selected phase. If a solution can be found, the Euler angles can be calculated, thus determining the orientation. Nowadays, other methods could be used to index a pattern as the dictionary one or much faster the so-called spherical indexing method, what will be describe in another chapter.

In parallel to this work and for several years, Dingley, in particular, worked on the symmetries of diffraction images and Michael using the signal from an EDS detector in order both to improve the identification of unknown phases [28-29-30]. The later idea was to acquire an EDS spectrum to get the chemistry and then select phases corresponding to that chemistry to index a pattern.

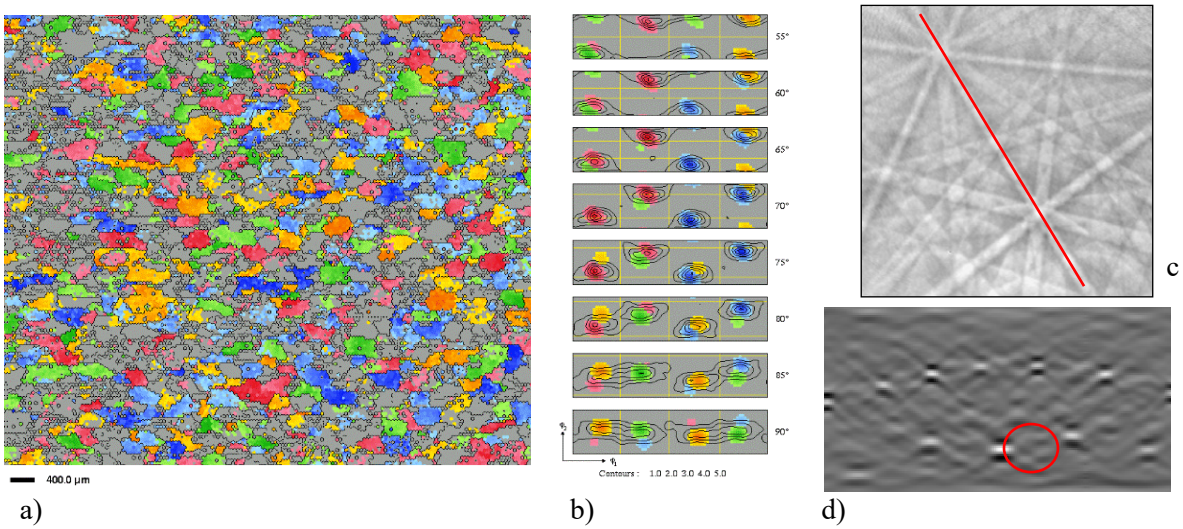

Figure 8. a) One of the first OIM maps on a 40 % compressed aluminium acquired on February 4, 1992; b) Selected grains on the map; c) A pseudo-Kikuchi pattern in real space; d) The Hough space corresponding to the pattern presented in c). The red line in c) correspond to the peak in d).

In 1996, Field and Wright could present the first multi-phase maps using the stage scanning mode, (Fig. 9a) [31] and Wright to further develop his algorithm in order to perform the first simultaneous EBSD-EDS acquisitions in 1997 on an automatic system (Fig. 9b) [32].

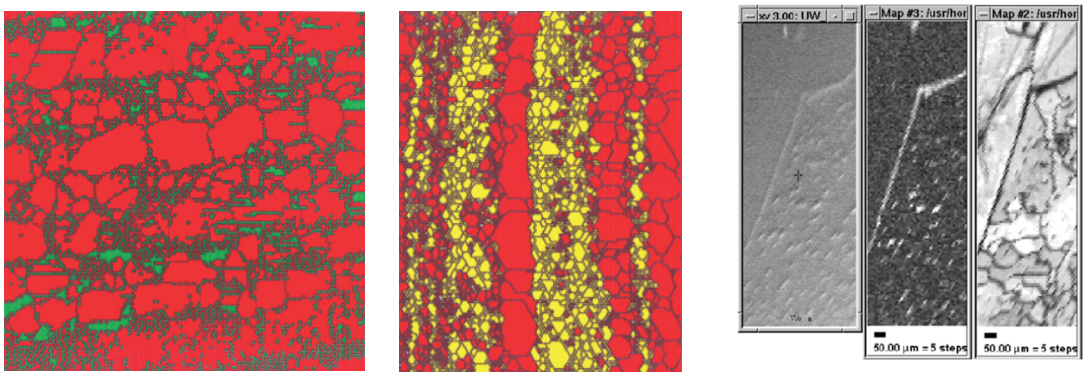

a) b) c)

Figure 9. a) One of the first multi-phase maps (austenite grains in bands between ferrite grains, 0.5 µm); b) multi-phase mapping TiAl-Ti_3Al; c) One of the first simultaneous acquisitions EBSD-EDS made in 1997 (secondary electron signal, EDS Ni-Kα, EBSD-IQ index).

5. *CAMERAS*

Since the introduction of EBSD technology in SEM and until today, various cameras have been used. There were TV, SIT, SIT-type cameras with fibre optic coupling, analogue CCD cameras and then cameras with digital CCD sensors. Currently, digital CCDs are used but CMOS cameras (see below) are taking over thanks to their speed and sensitivity. At the same time, direct detection cameras have recently appeared in EBSD. Back to the CCD cameras, their resolution has tended to decrease from a resolution of the order of 1000 × 1000 pixels or more, to a video format of 640 × 480 pixels, except for very specific applications (e.g., EBSD at high angular resolution). Thus, in the vast majority of cases, the resolution of the pattern used for the calculation of the Hough transform is of the order of 100 × 100 pixels. It is, therefore, unnecessary to use an image resolution of 1000 × 1000 pixels, or even more. This step of "degrading" the resolution is called "binning". It involves grouping adjacent pixels together (2 by 2 or 4 by 4, etc.). This has two effects: one to decrease the resolution of the captured pattern and the other to increase the signal of the new "large" pixel and thus the signal-to-noise ratio, which is usually very interesting. This results in a much higher reading speed of the CCD sensor and a correspondingly reduced acquisition time for the same quantity of electrons arriving on the sample. Note that the announced speeds often correspond to specific acquisition conditions and in particular "binning". It should also be noted that the maximum possible acquisition speeds, in reality, depend on many parameters, such as the high voltage of the incident electrons, the probe current, the quality of the sample, the surface preparation of the sample, the camera settings, the calculation parameters of the Hough transform, ...

Thus, EBSD camera models have evolved greatly from the first systems to the present day, moving from TV cameras, SIT to CCDs. This has made it possible to acquire data more and more quickly and to optimise performance [33, 34]. Table 1 below shows a comparison of the different models of the "same" camera type between 1990 and 2011. This table compares, for example, the acquisition times of a map of one million points over time, or rather the time it would have taken to acquire a million points from the beginning of analogue CCD cameras to the latest fast digital CCD cameras. In this table some data from CMOS cameras have been added. The advantage of this last type of sensor and electronic lies in the parallel lecture of the ships. At the end, they allow to work 10 times faster than the fastest CCDs for the same SEM settings and sample. Such a factor is so important that most of the systems are now sold with this type of sensors.

Table 1. Type of cameras and acquisition time to acquire 1 million points.
(CCD data, from NORDIF EBSD cameras J. Hjelen).

Year	Number of patterns acquired per second	Acquisition time
CCD analogue:		
1990	10 s./pattern semi-automatic	
1995	3 s./ pattern, automatic	35 days
1999	3 pattern/s.,	4 days
2000	10 pattern/s.,	
2001	20 pattern/s.,	
CCD digital:		
2002	40 pattern/s.,	7 hours
2007	750 pattern/s	22 minutes
2009	1000 pattern/s	
2011	1170 pattern/s	14 minutes
CMOS:		
2018	3000 pattern/s	
2022	6700 pattern/s	2.5 seconds

High-speed cameras are particularly interesting in the case of in-situ tests, for example in temperature. Indeed, let us imagine a recrystallisation test: If the acquisition time of an EBSD map is too long, the transformations take place, not only during the increase in temperature but also during the acquisition of the EBSD map at constant temperature, making the analysis of the data more problematic. However, there are many other cases where gaining in acquisition speed is interesting. In particular, if a microscope other than a Schottky-SEM is used, reducing the acquisition time thus reduces the risk of a variation in beam intensity, instability of the electron beam or filament rupture (W-SEM).

All the cameras mentioned above were equipped with a sensor, an optical system for focussing and a phosphorescent screen. This screen made it possible to image the diffraction image emitted

by the sample at a given point in the sample, which was recorded by the sensor. In direct-detection cameras, this screen and the optical transfer system no longer exist and the signal arrives directly on the sensor. This makes it possible to detect, without loss, a single electron and there is no longer any distortion related to the optical system. Even though a few laboratories have been testing such cameras since the 2010s to acquire EBSD patterns [35-37], their commercial introduction only began in 2020 in EBSD. while they had been used for more than 10 years in TEMs. As these cameras are extremely sensitive, it is possible to use low voltages, up to 3 kV, and especially beam currents of very low intensity, up to ten pA, whereas currents of the order of nA or some 10 nA are usually used with CCD and CMOS cameras. This makes it possible to carry out orientation maps on extremely sensitive materials, such as perovskites used for solar cells, by example.

6. ON THE EDGE OF THE CLASSICAL EBSD

6.1. Some other contrasts

Since the late 1990s, it has been possible to acquire the signal from secondary electrons (SE) from the Everhart-Thornley detector or possibly the conventional backscattered electron (BSE) detector within the interface of the EBSD software, for example to help to place the area to be acquired (Fig. 10). Nevertheless, the first detector gives very little crystallographic contrast (Fig. 10b) and the second is very poorly positioned to recover the signal corresponding to the backscattered electrons, since it is placed under the polar piece and the surface of the sample to be analysed is inclined by 20° with respect to the axis of the incident beam (Fig. 10c). Thus, in order to obtain a contrast of orientation, a detector can be installed in front of the EBSD camera and it is usually called FSD (forescatter detector), this is the most common solution (Fig. 10e). It is also possible to use a sample current detector integrated into a pre-inclined sample holder. This solution is rarer, yet the signal generates relatively high-contrast images (Fig. 10d). Thus, these last two detectors are very efficient and give crystallographic-like contrasts, similar to that of a conventional BSE detector.

However, another solution has been considered [38-39]; It involves using the intensity of the electronic signal obtained at each point of acquisition of an EBSD scan and coming from specific areas of the phosphorescent screen. This signal can be called a virtual FSD and an example of an image reconstructed in this way is given in Fig. 11. The use the camera screen as an electron detector, or virtual FSD detector is used like shown on Fig. 11a. Areas can be selected to create and image. The very interesting point is that depending on the selected area, you can have very different images. The top area can give an image related to chemistry, the central area an image looking like the FSD detector and the bottom area a topographic image. Of course, the contrast varies depending on the sample. Figs. 11b and 11c are issued from an Ag soldering sample that has been ion polished to give a lot of relief and are of exactly the same area.

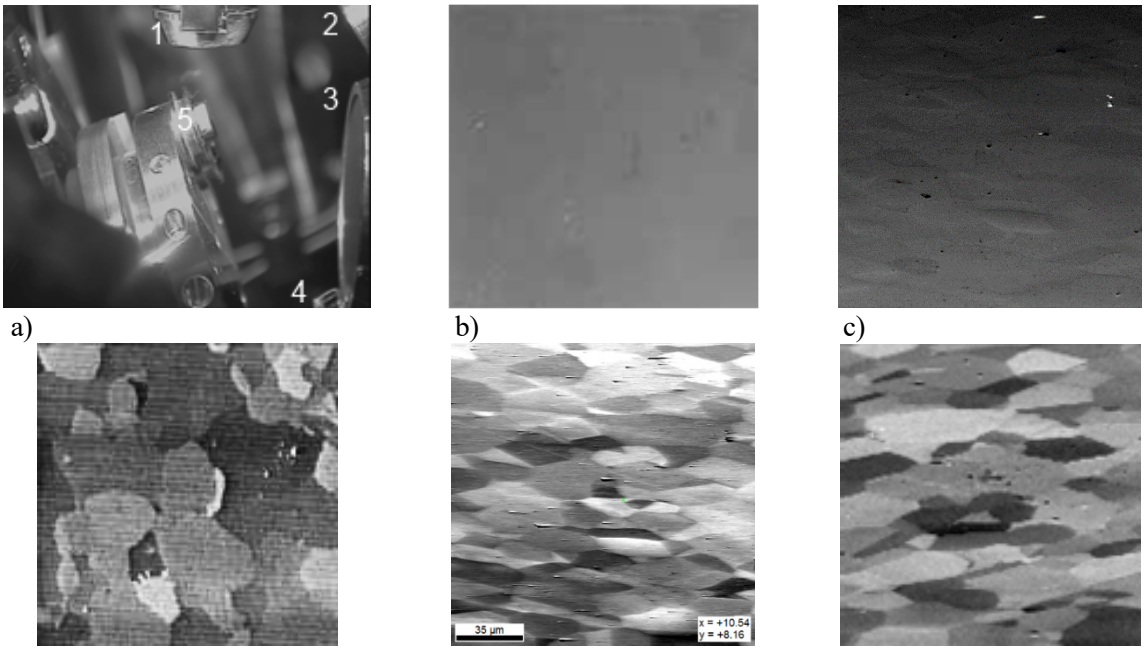

a) b) c)

d) e) f)

Figure 10. a) SEM chamber and detectors; b) SE signal; c) Classical BSE signal; d) Sample current signal; e) FSD signal; f) Virtual FSD signal; from b) to f) the images are obtained from a recrystallised Ni. In a): 1) BSE detector, 2) EDS detector, 3) EBSD camera screen, 4) FSD detector, 5) sample, the SE detector is located behind the EDS detector, it is not visible in this image.

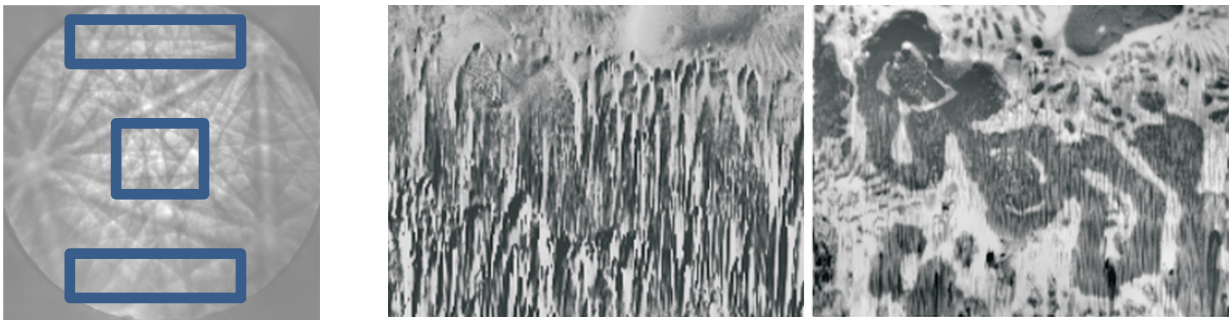

a) b) c)

Figure 11. a) Screen of the camera and areas for virtual FSD; b) Image from the bottom area; c) Image from the top area [from 38], a similar function is called PRIAS in the EDAX software.

6.2. EBSD and EDS combined analyses

Long before EBSD reached its current level of development, work was undertaken to combine EBSD with EDS, as previously mentioned (Fig. 9c). And indeed, the first combined analyses date back to 1996-1997. There were three main reasons for this development. On the one hand, EDS is a well-known technique, very well established on SEMs and it is certainly the most widespread analysis system on microscopes. On the other hand, this technique can help to

identify the phases involved. This can be achieved manually with the acquisition of an EDS spectrum followed by quantitative analysis or automatically by a simultaneous EBSD acquisition. The processing of experimental data then varies according to the manufacturer. These range from the simple simultaneous acquisition and then the superimposition of EDS and EBSD information, to the actual processing of the data and the use of the EDS to select the phase to be used during indexing. In addition, there are cases where the crystallographic identification of multiple phases can be compromised. Indeed, the basic principle of Hough indexing is to measure the angles between the bands of a Kikuchi pattern in order to find the right phase and index the pattern. If the sample contains, for example, two phases of the centred cubic type, independent of the crystal parameter, the angles between the bands (the hkl-plane families) will be the same. Thus, in such a case, the EDS can help select the correct phase. EDS and EBSD can also sometimes be used sequentially. The system acquires an EBSD pattern and an EDS spectrum. The latter is quantitatively analysed and the system chooses from a database the crystallographic phases that can correspond to this analysis. Only these phases are indexed and the system then selects the right phase. The latter technique can be used to identify unknown phases, but is not widely used, as it is difficult to implement effectively. Indeed, a quantitative analysis at 70° inclination must be carried out, and there can be a fairly large number of phases that can correspond to a given quantitative analysis.

As an example, Fig. 12a shows the mapping of the orientations of a nickel deposit made by laser cladding on a copper-aluminium substrate [40]. Since the cfc crystal structures are the same for nickel, copper and aluminium and the lattice parameters are close, it is not possible to dissociate the different phases during a classical EBSD analysis. On the other hand, taking into account the chemistry (Fig. 12b) in the procedure for indexing Kikuchi diagrams, the phase distinction can be made perfectly (Fig. 12c – left and 12c – right). This coupling also revealed an impurity of γ-iron (also of CFC structure) in nickel. Note that the deposition conditions were not poorly chosen, detachment of the deposit, tearing of the substrate and cracking in the substrate appears.

6.3. t-EBSD or TKD

The technique that makes it possible to diffract an object, no longer massive, but thin in transmission mode in a SEM is referred to by the acronym TKD (Kikuchi diffraction transmission) and sometimes also by the acronym t-EBSD (transmission electron backscatter diffraction). (Remark: The terms used to refer to the technique and the acronyms derived from it, whether it is "EBSD in transmission mode (t-EBSD)" or "Kikuchi diffraction in SEM transmission (TKD)", are not the most appropriate. Indeed, the electrons that form the diffraction pattern are electrons that have scattered with angles less than 90°, so they are not strictly speaking backscattered electrons. Moreover, as we will see later in the TKD on-axis section, we obtain not only diagrams made up of lines or bands, called Kikuchi diagrams, but also diagrams made up of points. It would therefore have been preferable to speak of transmission diffraction in SEM (transmission diffraction TD in SEM). Nevertheless, the term TKD was later used because it had now been consecrated by usage). It is a relatively recent technique since it was first proposed

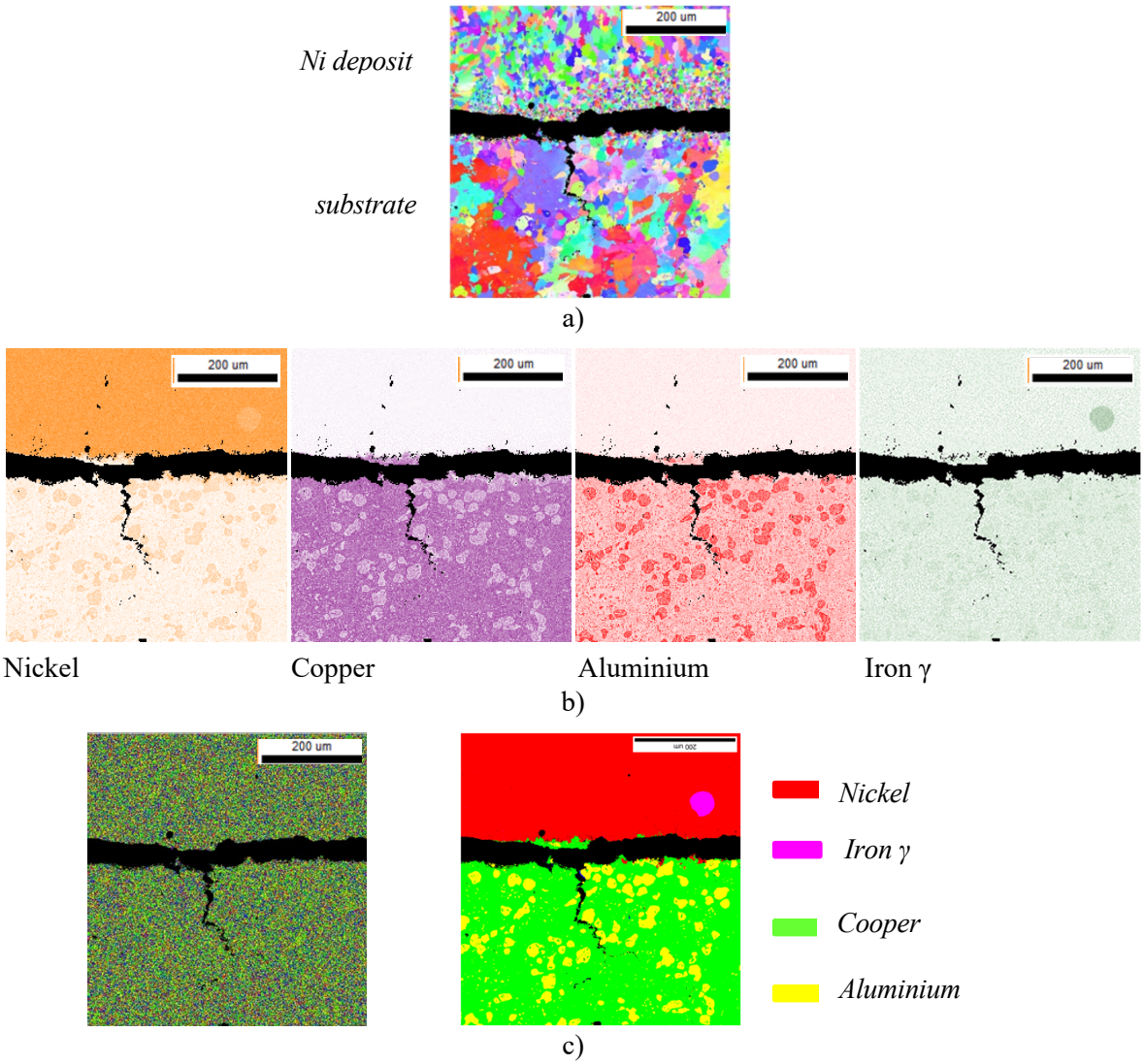

Figure 12. Nickel deposit on a copper-aluminium substrate; a) Mapping of {*hkl*} planes // observation plane; b) EDS maps of the different elements; c) EBSD mapping of phases without using the chemical filter on the left and using the chemical filter on the right.

and implemented by Keller *et al.* in 2012 [41]. In a few years, it has become increasingly successful [42, 44]. The main reason for this craze is that it makes it possible to carry out orientation maps with a spatial resolution of the order of a few nanometres. The EBSD technique, which is now very commonly used in Materials Science, Geology, etc., is often limited to a spatial resolution of a few tens of nanometres, even if it is sometimes possible to go down to 20, 10 or even 5 nm for more favourable samples (very good backscatter coefficients, for example, Fig. 13). The TKD technique appears to be its ideal complement to characterise ultra-fine-grained materials or nanocrystalline materials and should make it possible to overcome the resolution limitations observed in classical EBSD and also be applicable to more materials. It should thus make it possible to reduce the value of the acquisition step (Fig. 14) and to achieve a lateral resolution of up to the nanometre. The other reason is that it is quite easy to implement. Indeed, the diffraction patterns are collected by the scintillator + camera assembly of the EBSD

system and they are then analysed to determine the phases, the orientation of the grains using the software that has been developed for EBSD. In short, it is enough to have a sample holder suitable for thin samples to implement the TKD technique, even if there are more sophisticated solutions at the present time.

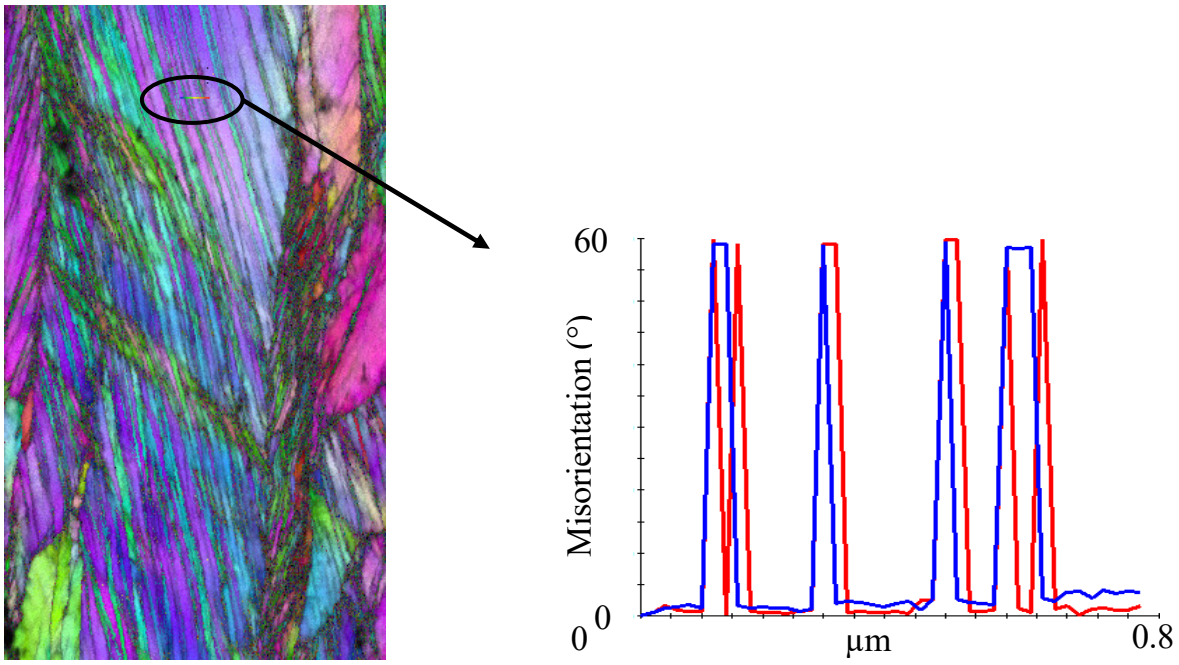

a) b)

Figure 13. a) EBSD IPF map acquired with a 20 nm step, map width 10 µm; b) Misorientation graph.

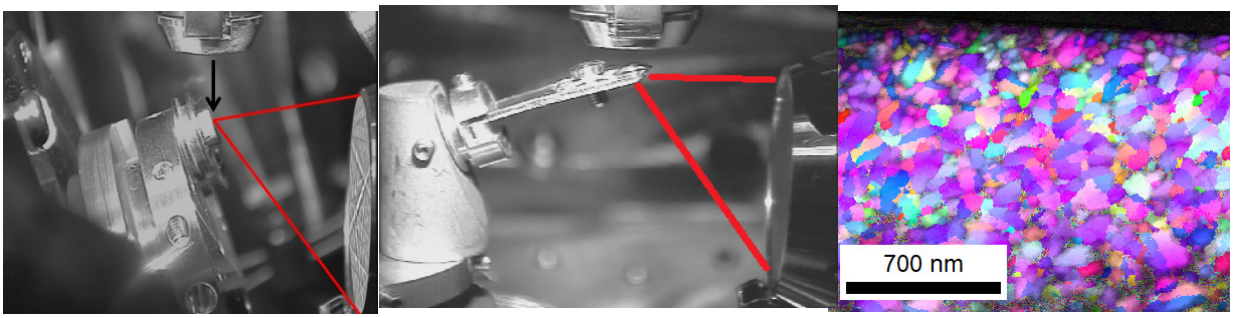

a) b) c)

Figure 14. a) Classical EBSD setup; b) Historical TKD setup at the laboratory; c) IPF map acquired in TKD mode, 30 kV, 120 µm aperture, high currant mode, 100 pts/sec, step 5 nm.

Figure 15 shows maps of a steel acquired with a step of 10 nm. It highlights both the matrix and the main precipitates based on chromium and titanium. The black areas on the right in the images correspond to the edge of the slide. Points with a CI confidence index < 0.05 have been removed,

they probably correspond to other smaller precipitates not analysed. Figs. 15a to 15c correspond to the maps related to the quality of the images (quality index), orientation and phases, respectively, while the following images, Figs. 15d to 15g, represent the chemical maps. The gain in resolution in EDS is very well highlighted here, compared to a massive sample. The EDS and EBSD resolutions then become similar.

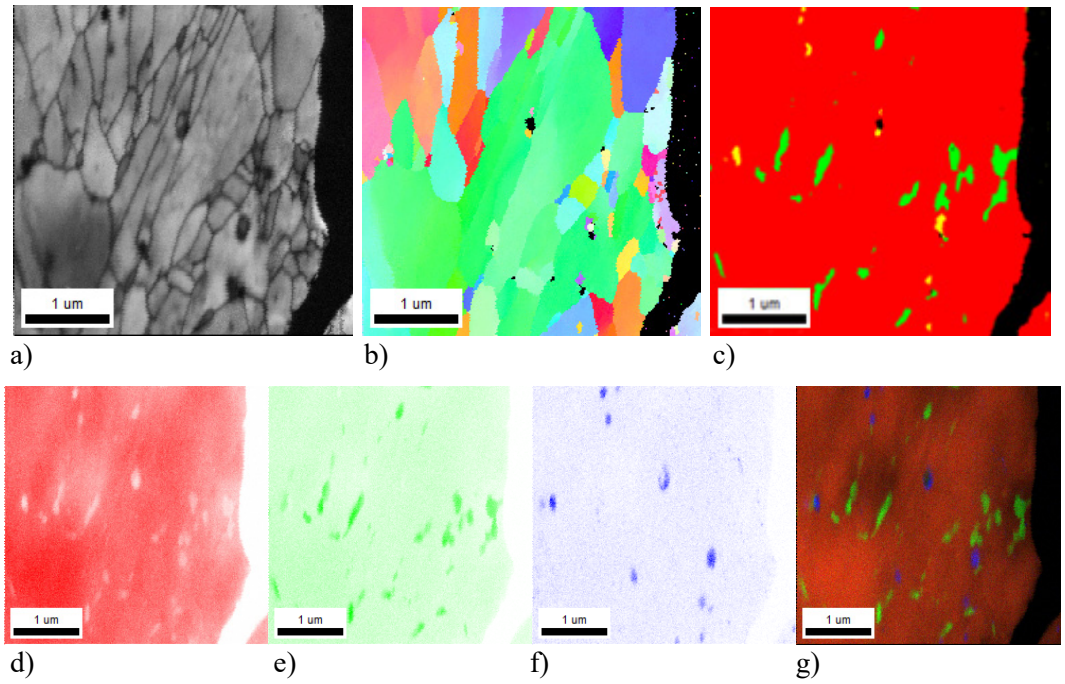

Figure 15. Iron alloy thin foil maps: a) IQ; b) IPF; c) Phases (red Fe_{α}, green $Cr_{23}C_6$ and yellow TiO_2); d) EDS Fe; e) EDS Cr; f) EDS Ti; g) EDS Fe+Cr+Ti; acquisition step 10 nm; HT 30 kV, map duration 15 minutes; map resolution 300 × 300 points, 100 pts/s.

6.4 3D EBSD

No sooner had EBSD been fully established as a powerful analytical technique for a large number of materials than studies were carried out, not only to obtain data in two dimensions, but also in three dimensions. Produced with double-column equipment, the SEM-FIB or by successive manual polishings, the EBSD-3D [45-47] was born. The data obtained can then be represented in the form of a "data cube" and be processed by visualisation programmes (Fig. 16). Thus, it is possible to image individual grains, isolate them, etc. Many developments are currently underway to try to extract information about grain boundaries, for example, and not just give nice graphical representations. A chapter will be dedicated to this particular development, detailing some aspects of it.

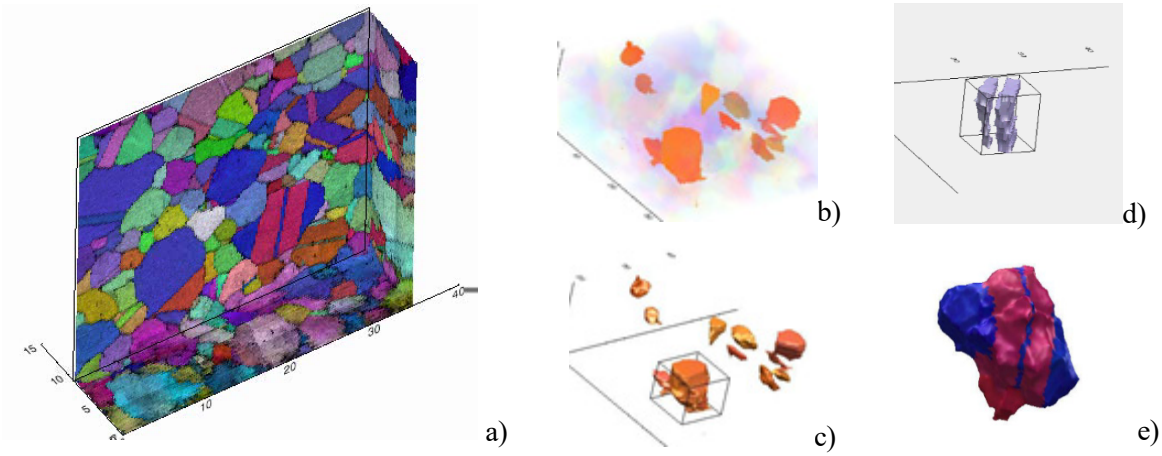

Figure 16. a) Reconstruction of an EBSD data cube following the acquisition of multiple 2D EBSD maps from an ion abrasion; b-e) Various representations from a 3D reconstruction: b) visualisation of grains of particular orientation, and c) extraction of these grains; d) Visualisation of a twin, and e) extraction of a twin grain.

6.5 Deformations and residual stresses

In parallel with the classical EBSD analyses developed since the very beginning of the 1990s, Wilkinson and Dingley have been closely interested in the characterisation of deformations in materials, then in elastic and residual stress measurements, since 1991 [48-49]. This measurement is all the more difficult because it is already necessary to be able to overcome a deformation linked to the preparation of the samples. Once this pitfall has been overcome, it is necessary to be able to determine the absolute orientation very precisely in order to be able to obtain significant and often very weak point-by-point disorientations. Substantial work was, therefore, undertaken and led to many recognised communications and developments [50-52]. One of the important points of this measurement is therefore the positioning of the centre of the image, called the "pattern centre" and the principle of this specific analysis technique is based on the comparison of EBSD images from distorted areas with respect to a "control" image considered as undistorted. The analysis is carried out by cross-correlation of images on specific areas of these images (Fig. 17).

An in-depth chapter of this book will describe the most significant principles and advances related to this emerging technique.

7 CONCLUSION

EBSD has now reached a recognised level of maturity, whether used alone or in combination, for example with EDS. However, it is important to remember that it is a surface analysis technique and that the data obtained may not be representative of the entire material or may be subject to artifacts related to sample preparation. In the first case, it may be beneficial to combine

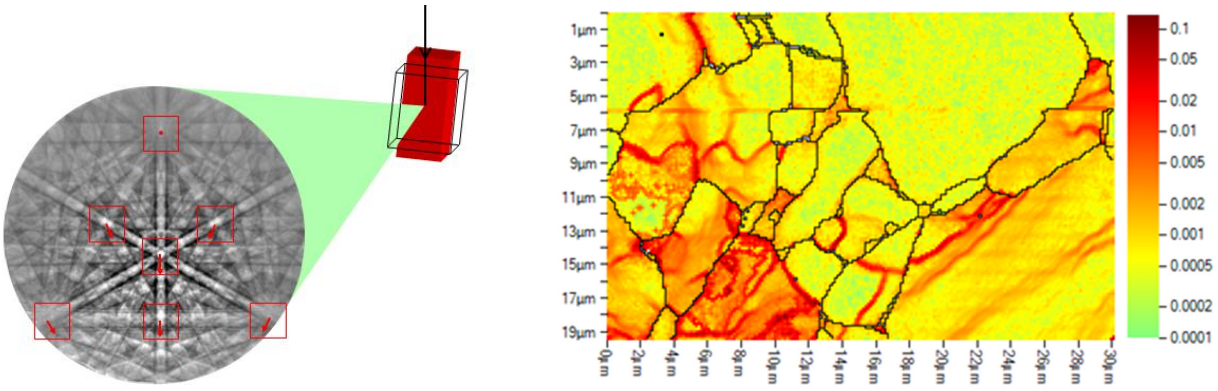

a) b)

Figure 17. a) Example of regions of interest taken from a Kikuchi diagram, and b) Misorientation map in HR-EBSD [50].

the analyses with X-ray and/or neutron diffractions which have much larger interaction volumes. In the second case, numerous preparation methods have been developed over the years depending on the different types of samples, ranging from classical polishing techniques to ion beam techniques. I recommend reading the chapter dedicated to that topic in this document.

8. *ACKNOWLEDGEMENTS*

Special thanks to Stuart Wright who, by delving back into his archives from the last 30 years rediscovered the historical images of his first OIM orientation maps and therefore offered them for this article. My sincere thanks to David Dingley, with whom I began my work on EBSD as well as to Jarle Hjelen, René de Kloe, Graham Meaden, my colleagues Thierry Baudin, Denis Solas, Anne-Laure Helbert, Daniel Monville, Dominique Loisnard, and many others for so many invaluable exchanges over the years, and for sharing a common enthusiasm for this microstructural analysis technique.

9. *REFERENCES*

[1] Davisson C J and Germer L H 1927 *Nature* **119** 558
[2] Thomson G P 1928 *Proc. Roy. Soc. Ser. A* **117** 600
[3] Kikuchi S 1928 *Proc. Imp. Acad. Jap.* **4** 354
[4] Nishikawa S and Kikuchi S 1928 *Proc. Imp. Acad. Jap.* **4** 475-477
[5] Meibom R and Rupp E 1933 *Z. Phys.* **82** 690
[6] Boersch H 1937 *Physik. Zeitschrift* **38** 1000-1004
[7] Alam M N, Blackman M and Pashley D W 1954 *Proc. Royal Soc. London A* **221** 224-242
[8] Coates D G 1967 *Phil. Mag.* **16** 1179

[9] Joy D C and Booker G R 1971 *J. Phys. E* **4** 837
[10] Biggin S and Dingley D J 1977 *J. Appl. Cryst.* **10** 273
[11] Venables J A and Harland C J 1973 *Phil. Mag.* **2** 1193-1200
[12] Dingley D J 1975 Scanning electron microscopy. (Johari O and Corvin I; Eds.) [Chicago, IL: IIT Research Institute]
[13] Venables J A and Bin-Jaya R 1977 *Phil. Mag.* **35** 1317-1321
[14] Joy D C, Booker G R, Fearon E D and Bevis M 1971 *Quantitative crystallographic orientation determinations of microcrystals present on solid specimens using the SEM*. in: Proc. 4th Ann. Scanning Electron Microscopy Symp. [Chicago, IL: IIT Research Institute], 497-504
[15] Dingley D J 1981 *Scanning Electr. Microsc.* **4** 273-286
[16] Dingley D J 1984 *Scanning Electr. Microsc.* **11** 569-575
[17] Dingley D J, Longdon M, Wienbren J and Alderman J 1987 *Scanning Microscopy* **1** 2
[18] Dingley D J 1990 *Development in on-line crystal orientation measurement.* in: Inst. of Physics Conf. Series, EMAG. [London and Bristol, UK: Institute of Physics] 473
[19] Dingley D J, Randle V and Baba-Kishi K Z 1994 *Atlas of backscattering Kikuchi diffraction patterns*. [Bristol, U.K. and Philadelphia, PA: Institute of Physics Publishing]
[20] Schmidt N H and Olesen N Ø 1989 *Can. Mineralogist* **27** 15-22
[21] Jeesen D J and Schmidt N H 1991 *Texture, Stress & Microsctructures* **14-18** 97-102
[22] Wright S I and Adams B L 1992 *Met. Trans. A* **23** 759-767
[23] Burns J B, Hanson A R and Riseman E M 1986 *IEEE Trans. Pattern Analys. Machine Intelligence* **8** 425-455
[24] Hough P 1962 *Method and Means for Recognizing Complex Patterns*. Brevet US 3 069 654
[25] Wright S I 1992 *Individual lattice orientation measurements development and applications of a fully automatic technique*. PhD-Thesis. [New Haven, CT: Yale University]
[26] Krieger-Lassen N C, Conradsen K and Juul-Jensen D 1992 *Scanning Microscopy* **6** 115-121
[27] Kunze K, Wright S I, Adams B L and Dingley D J 1993 *Textures Microstructures* **20** 41-54
[28] Dingley D J and Baba-Kishi K 1986 *Scanning Electron Microscopy* **1986** (2) 383-391
[29] Dingley D J, Mackenzie R and Baba-Kishi K 1989 *Application of backscatter Kikuchi diffraction for phase identification and crystal orientation measurements in materials*. in: Microbeam Analysis. (Russell P E; Ed.) [San Fransico, CA: San Francisco Press] 435-436
[30] Michael J R and Goehner R P 1993 *MSA Bulletin* **23** 168-175
[31] Field D P, Wright S I and Dingley D J 1996 *Multiphase texture analysis by orientation imaging microscopy*. in: 11th Int. Conf. on Textures of Materials. (Xian, P.R. China) [Beijing, P.R. China: Int. Conf. Publ.] 134
[32] Wright S I and Field D P 1997 *Microsc. Microanal.* **3** 561-562
[33] Søfferud M, Hjelen J, Karlsen M, Dingley D and Jaksch H 2008 *Future prospects on EBSD speeds using a 40 nA FESEM*. in: EMC 2008 (Aachen, Germany) 625

[34] Chen Y, Hjelen J, Gireesh S and Roven H J 2011 *J. Microscopy* **245** 111-118
[35] Wilkinson A J, Moldovan G, Britton T B, Bewick A, Clough R and Kirkland A I 2013 *Phys. Rev. Lett.* **111** 065506
[36] Vespucci S, Winkelmann A, Naresh-Kumar G, Mingard K P, Maneuski D, Edwards P R, Day A P, O'Shea V and Trager-Cowan C *Phys. Rev. B* **92** 205301
[37] Nowell M, de Kloe R and Wright S 2021 *Microsc. Microanal.* **27** (Suppl. 1), 3434
[38] Schwarzer R, Sukkau J and Hjelen J 2011 *Imaging of topography and phase distributions with an EBSD detector in the SEM*. in: Microscopy Conference (Kiel, Germany)
[39] Wright S I, Nowell M M, de Kloe R, Camus P and Rampton T 2015 *Ultramicroscopy* **148** 132-145
[40] Brisset F, Ndzana T, Bourahima F, Helbert A L and Baudin T 2016 *Glass mould loading optimization by laser cladding. Microstructure and internal stress studies based on process parameters*. in: EMAS 2016 Book of Tutorials and Abstracts. [Antwerp, Belgium: EMAS] ISBN 978 90 8227 692 3
[41] Keller R and Geiss R H 2012 *J. Microscopy* **245** 245
[42] Rice K P, Geiss R H and Keller R R 2013 *Transmission electron backscatter diffraction in the SEM: Specimen thickness effects*. in: 2013 FCMN (Gaithersburg, MD: NIST)
[43] Suzuki S 2013 *J. Microscopy* **65** 1254-1263
[44] Brodusch N, Demers H and Gauvin R 2013 *J. Microscopy* **250** 1-14
[45] Zaefferer S 2005 *Mater Sci Forum* **495-497** 3-12
[46] Zaafarani N, Raabe D, Singh R N, Roters F and Zaefferer S 2006 *Acta Materialia* **54** 1863
[47] Zaefferer S, Wright S and Raabe D 2008 *Metall. Mater. Trans. A* **39** 374-389
[48] Wilkinson A J and Dingley D J 1991 *Acta. Metall. Mater.* **39** 3047
[49] Wilkinson A J 1996 *Ultramicroscopy* **62** 237
[50] Wilkinson A J, Meaden G and Dingley D J 2006 *Ultramicroscopy* **106** 303
[51] Maurice C, Driver J H and Fortunier R 2012 *Ultramicroscopy* **113** 171-181
[52] B. Britton, I. Holton, G. Meaden, D. Dingley 2013 *Microsc. Analysis* **98** 8-13